Wavelength-stabilized figure-of-9 thulium-doped all-fiber laser emitting 560 fs pulses

OPEN ACCESS
IOP Publishing | Astro Ltd
Laser Physics
Laser Phys. **34** (2024) 025101 (7pp)
https://doi.org/10.1088/1555-6611/ad1504

Wavelength-stabilized figure-of-9 thulium-doped all-fiber laser emitting 560 fs pulses

Moritz Bartnick[1,*], Gayathri Bharathan[1,2], Thorsten A Goebel[3,4], Ria G Krämer[3], Stefan Nolte[3,4] and Camille-Sophie Brés[1]

[1] École Polytechnique Fédérale de Lausanne (EPFL), Photonic Systems Laboratory (PHOSL), Lausanne CH-1015, Switzerland
[2] Indian Institute of Technology Delhi (IITD), Optics and Photonics Centre (OPC), New Delhi IN-110016, India
[3] Friedrich-Schiller-Universität Jena, Institute of Applied Physics, Abbe Center of Photonics, Albert-Einstein-Str. 15, Jena D-07745, Germany
[4] Fraunhofer Institute for Applied Optics and Precision Engineering IOF, Center of Excellence in Photonics, Albert-Einstein-Str. 7, Jena D-07745, Germany

E-mail: moritz.bartnick@epfl.ch

Received 13 October 2023
Accepted for publication 8 December 2023
Published 22 December 2023

Abstract

We demonstrate a figure-of-9 all-fiber thulium-doped laser (TDFL) that generates 560 fs long pulses at 1948 nm wavelength. In order to achieve self-starting passive mode-locking, we utilize an in-fiber Faraday rotator to induce a nonreciprocal phase shift. To the best of our knowledge, this is the first all-fiber TDFL that combines an artificial saturable absorber (SA) with a chirped fiber Bragg grating (CFBG) as a wavelength-selective reflector. This cavity design is an excellent candidate to pump nonlinear processes such as supercontinuum and frequency comb generation since it does not require any SA material that degrades over time for mode-locking and could be made wavelength-tuneable via the CFBG.

Keywords: thulium-doped fiber laser, figure-of-9, nonlinear amplifying loop mirror (NALM), nonreciprocal phase shifter, chirped fiber Bragg grating (CFBG)

1. Introduction

Higher orders of molecular vibrations overlap with the 2 μm spectral region, and a wide variety of atmospheric constituents, including NH_3, NO_2, CO_2 and H_2O, can therefore be directly detected in the 2 μm spectral band [1, 2]. While mid-infrared (MIR) spectroscopy targets even stronger absorption lines, its implementation requires rather complicated setups for the generation [3], as well as the detection [4], of MIR light. On the contrary, the 2 μm band is more easily accessible since this wavelength can be obtained directly from Tm^{3+}-doped active silica fibers, and detected by InGaAs photodiodes [5]. To utilize the advantages of fiber laser systems, which include their scalability and robustness against environmental influences, we developed a thulium-doped fiber laser (TDFL) that generates 560 fs long pulses at 1948 nm wavelength.

Mode-locked lasers utilizing various saturable absorber (SA) materials, such as semiconductor SA mirrors (SESAMs) [6], carbon nanotubes (CNTs) [7, 8], or graphene [9], are well-established. These materials are particularly useful since they enable mode-locked lasers to

* Author to whom any correspondence should be addressed.

self-start [10], but they also deteriorate with time [11–13]. Artificial SAs, devices that exhibit lower optical losses for higher intensities, but without actual absorption, are thus a viable alternative to SA materials. They are especially useful for the generation of fs-pulses since they are based on nonlinear effects and belong to the fast SAs [10]. To implement a mode-locked laser based on an artificial SA, nonlinear polarization rotation (NPR) can be exploited. While this technology is simple and direct, NPR lasers are susceptible to ambient factors and cannot be fully polarization-maintaining (PM) intrinsically [10, 14]. Alternatively, a nonlinear amplifying loop mirror (NALM) can be used as an artificial SA. A NALM consist of a 2 × 2 fiber optical coupler in combination with an active fiber, described in further detail in section 2.1. NALMs can be integrated into figure-of-8 and figure-of-9 laser cavities. Figure-of-8 cavities are difficult to start on their own. To enter a passively mode-locked regime they require, for instance, an electro-optic modulator [15], extremely careful regulation of cavity dispersion and nonlinearity [16], or a 3 × 3 instead of a 2 × 2 optical coupler [17], which contributes additional loss to the laser cavity. In our work, we present a figure-of-9 cavity, since this architecture allows for the integration of retroreflectors to stabilize the emission wavelength and manage the cavity dispersion [11]. For self-starting, figure-of-9 cavities can include a nonreciprocal phase shifter (NRPS) [18]. In 1994, Lin *et al* proposed implementing this component by combining two Faraday rotators (FRs) with a half-wave plate [19], which is still a common technique today [20–23]. To date, demonstrations of TDFLs based on NALMs therefore still include free-space half-wave plates and FRs [22, 23] or include SA materials to initiate mode-locking [24].

In this article, we present a true all-fiber TDFL based on a NALM as an artificial SA. We use an in-fiber Faraday-rotator in conjunction with a fiber optic polarization controller (PC) to create a nonreciprocal phase shift. We stabilize the emission wavelength at 1948 nm using a chirped fiber Bragg grating (CFBG) and achieved a pulse duration of 560 fs. To the best of our knowledge, this is the first all-fiber TDFL that incorporates an artificial absorber and a wavelength-selective CFBG. The laser design we propose avoids the possible deteriorating SA material, paving the way for the implementation of a robust pump source for supercontinuum and frequency comb generation.

2. Theory

2.1. NALM

A NALM is an artificial SA that operates in reflection and consists of a 2 × 2 fiber optic coupler in combination with a gain medium, such as an active fiber. In a 2 × 2 coupler with 50% splitting ratio, as shown in figure 1(a), two input light fields E_1 and E_2 are coupled such that the output fields E_3 and E_4 are given by [25]:

$$\begin{pmatrix} E_3 \\ E_4 \end{pmatrix} = \frac{1}{\sqrt{2}} \begin{pmatrix} 1 & i \\ i & 1 \end{pmatrix} \begin{pmatrix} E_1 \\ E_2 \end{pmatrix} \tag{1}$$

This implies that the two input waves are not only separated, but the portions transmitted from port 1 to port 4, and from port 2 to port 3 also undergo an additional 90° phase shift. To construct a NALM (without an additional phase shifter), the output ports of the 50/50 coupler are connected to an amplifier (such as a gain fiber), offset from the central point of the loop (see figure 1(b)). In this scheme, an input wave E_{in} divides into a clockwise and a counter-clockwise wave, E_{cw} and E_{ccw}. Both waves experience a linear gain g and recombine in the 50/50 coupler after a full roundtrip. At low input powers $P_{\mathrm{in}} \propto |E_{\mathrm{in}}|^2$, without any nonlinear effects, the two waves interfere constructively in the initial input port and destructively in the other arm of the coupler. This is due to the 90° phase shift (cf equation (1)) which turns the NALM into a complete reflector with 100% reflectivity. However, at higher power levels, this interference changes. As shown in figure 1(b), E_{cw} first gets amplified and then travels through the remaining optical fiber of length L, whereas E_{ccw} first travels through the same length of optical fiber and gets amplified afterward. As a result, the two waves acquire a distinct nonlinear phase, $\delta\phi_{\mathrm{cw,ccw}}$ from the optical Kerr effect [26]:

$$\delta\phi_{\mathrm{cw}} = \gamma L g P_{\mathrm{in}} \quad \text{and} \quad \delta\phi_{\mathrm{ccw}} = \gamma L P_{\mathrm{in}}. \tag{2}$$

The phase shift is nonreciprocal, resulting in a nonlinear phase difference $\Delta\phi_{\mathrm{NL}}$ proportional to the input power:

$$\Delta\phi_{\mathrm{NL}} = \gamma L (g-1) P_{\mathrm{in}}. \tag{3}$$

This phase shift therefore has an impact on the loop reflectivity $R = |E_{\mathrm{r}}|^2/|E_{\mathrm{in}}|^2$. The graph in figure 1(c) was obtained using equations (1) and (3) and depicts the reflectivity as a function of input power $R(P_{\mathrm{in}})$ (see solid gray line). The reflectivity is 1 when $P_{\mathrm{in}} = 0$ and decreases as the input power increases. Because the reflectivity of a SA should rise as the power increases, the device in figure 1(b) cannot be utilized in this manner to achieve self-starting mode-locking [27]. To implement a self-starting mode-locked laser, a NRPS that adds another 180° phase shift to the nonlinear phase difference $\Delta\phi_{\mathrm{NL}}$ is required. In that case, the NALM reflectivity would increase together with the input power (see red dotted line in figure 1(c)). Because the intracavity power never reaches zero, the initial reflectivity is not zero either, thereby enabling the gradual buildup of a pulse within the cavity.

2.2. All-fiber NRPS

To realize an all-fiber phase-shifted NALM, we employ the scheme presented in figure 2(a), in which a 50/50 coupler is connected to an active fiber that is pumped using a wavelength-division multiplexer (WDM). A fiber-optic PC and an in-fiber 45° FR are added to the loop to create a 180° phase shift. To demonstrate that these two components can function as a NRPS, we investigate their influence on a forward and a backward traveling wave, which are both defined by their Jones vectors $\mathbf{E_1}$ and $\mathbf{E_2}$ (cf figure 2(b)). The single-mode (SM) active fiber and the FR's SM fiber pigtails may be arranged arbitrarily, resulting in uncontrolled birefringence. Their impact on

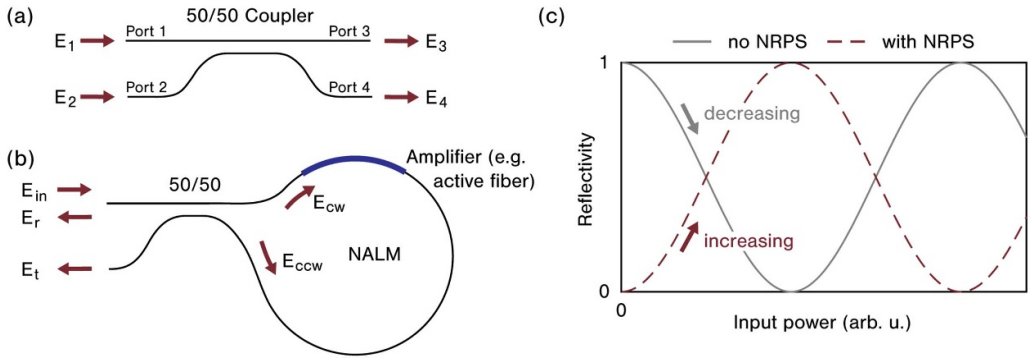

Figure 1. (a) Schematic of a 50/50 coupler, (b) schematic of a nonlinear amplifying loop mirror (NALM), (c) reflectivity as a function of input power without and with nonreciprocal phase shifter (NRPS).

a traveling wave is subsumed by a half-waveplate and quarter-waveplate, oriented at angles ϑ_1 and ϑ_2, respectively. The PC is represented by another waveplate pair set at angles θ_1 and θ_2, respectively. We describe the propagation of $\mathbf{E_1}$ and $\mathbf{E_2}$ through these components by their respective Jones matrices. The Jones matrix for a half-wave plate or quarter-wave plate oriented at an angle θ with respect to the horizontal x-axis are given by [11]:

$$M_{\mathrm{HWP}}(\theta) = e^{-i\frac{\pi}{2}} \begin{pmatrix} \cos^2\theta \sin^2\theta & 2\cos\theta\sin\theta \\ 2\cos\theta\sin\theta & \sin^2\theta - \cos^2\theta \end{pmatrix} \tag{4}$$

$$M_{\mathrm{QWP}}(\theta) = e^{-i\frac{\pi}{4}} \begin{pmatrix} \cos^2\theta + i\sin^2\theta & (1-i)\cos\theta\sin\theta \\ (1-i)\cos\theta\sin\theta & \sin^2\theta + i\cos^2\theta \end{pmatrix}. \tag{5}$$

The corresponding Jones matrix for the FR that rotates the polarization clockwise by an angle θ is [11]:

$$M_{\mathrm{FR}}(\theta) = e^{-i\frac{\pi}{4}} \begin{pmatrix} \cos\theta & -\sin\theta \\ \sin\theta & \cos\theta \end{pmatrix}. \tag{6}$$

We assume that the SM fibers are arbitrarily arranged, thus we choose random values for ϑ_1 and ϑ_2 (for the graphs shown later, we randomly selected $\vartheta_1 = 54.9°$ and $\vartheta_2 = 55.6°$). We assume equal input waves from both sides, and their polarization is determined by their amplitude in the x-direction A_x and the phase of the y-component φ.

$$\mathbf{E_1} = \mathbf{E_2} = \begin{pmatrix} A_x \\ \sqrt{1-A_x^2}\, e^{i\varphi}. \end{pmatrix} \tag{7}$$

By applying the Jones matrices in the corresponding order, we compute the Jones vectors of the transmitted waves $\mathbf{E_1'}$ and $\mathbf{E_2'}$. Since the backward traveling wave views the waveplates from a different perspective, the waveplate angles are negative in the second scenario.

$$\begin{aligned} \mathbf{E_1'} = {} & M_{\mathrm{QWP}}(\theta_2) M_{\mathrm{HWP}}(\theta_1) M_{\mathrm{FR}}(45°) \\ & \cdot M_{\mathrm{QWP}}(\vartheta_2) M_{\mathrm{HWP}}(\vartheta_1) \mathbf{E_1} \end{aligned} \tag{8}$$

$$\begin{aligned} \mathbf{E_2'} = {} & M_{\mathrm{HWP}}(-\vartheta_1) M_{\mathrm{QWP}}(-\vartheta_2) M_{\mathrm{FR}}(45°) \\ & \cdot M_{\mathrm{HWP}}(-\theta_1) M_{\mathrm{QWP}}(-\theta_2) \mathbf{E_2}. \end{aligned} \tag{9}$$

Our goal was to determine which combination of $(A_x, \varphi, \theta_1, \theta_2)$ meets the following two requirements. First and foremost, the forward and backward traveling waves should experience a 180° nonreciprocal phase shift. We therefore define the cost function Y_1, which must be zero when a 180° phase shift occurs.

$$Y_1 = \left| |\arg(\mathbf{E_2'} - \mathbf{E_1'})| - \sqrt{2}\pi \right| = 0. \tag{10}$$

For the second condition, the transmitted polarization should be the same as the input polarization. To account for this, we define the cost functions Y_2 and Y_3, both of which must be zero.

$$Y_2 = \left| \mathbf{E_1'} e^{-i\arg\left(E_{1,x}'\right)} - \mathbf{E_1} \right| = 0 \tag{11}$$

$$Y_3 = \left| \mathbf{E_2'} e^{-i\arg\left(E_{2,x}'\right)} - \mathbf{E_2} \right| = 0. \tag{12}$$

Finally, we define a total cost function Y that is zero when all the requirements are met.

$$Y(A_x, \varphi, \theta_1, \theta_2) = Y_1 + Y_2 + Y_3 = 0. \tag{13}$$

To identify the minima of $Y(Ax, \varphi, \theta 1, \theta 2)$, we used a standard gradient descent algorithm. We observed that for each SM fiber configuration $(\vartheta_1, \vartheta_2)$, there is one minimum in which $Y(A_x, \varphi, \theta_1, \theta_2) = 0$. For $\vartheta_1 = 54.9°$ and $\vartheta_2 = 55.6°$, for instance, we identified $Y(A_x = 0.71, \varphi = 0, \theta_1 = 68.2°, \theta_2 = 35.8°) = 0$ as the minimum.

Figure 2(c) shows a heat map of the total cost function Y when the PC setting is fixed at this point, while the input polarization is varied. Y is only minimal for $A_x = 0.71$ and $\varphi = 0$, i.e. for diagonal input polarization. In fact, when considering any other SM fiber birefringence $(\vartheta_1, \vartheta_2)$, we always observe that Y is only zero for diagonal input polarization. On the other hand, figure 2(d) shows a plot of the cost function Y for diagonal input polarization, but varied PC settings (θ_1, θ_2). Again, Y is only minimal in only one spot, i.e. for one PC setting. However, in this case, the location of this spot depends on the SM fiber birefringence $(\vartheta_1, \vartheta_2)$. Overall, we conclude that the assembly shown in figure 2(b) can function as a PM NRPS when the suitable PC setting is identified.

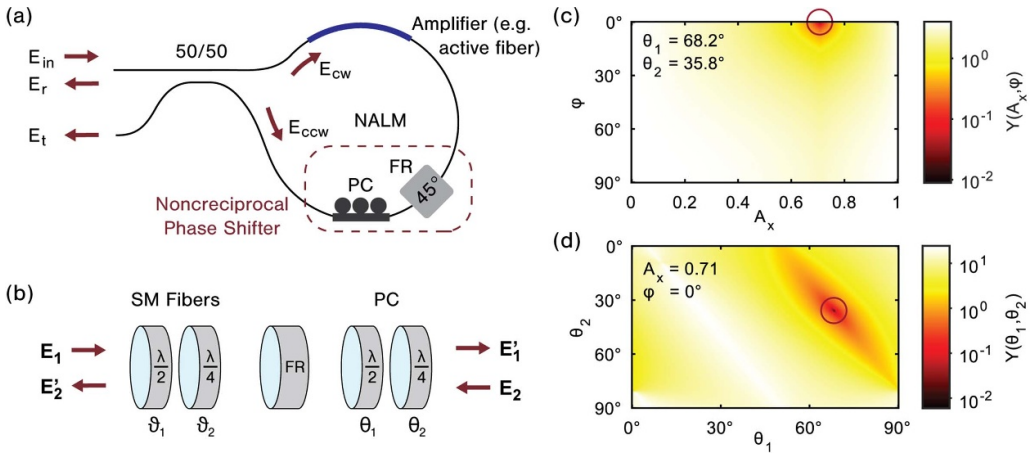

Figure 2. (a) Implementation of a nonreciprocal phase shifter in a NALM, (b) Fiber components represented by half- and quarter-waveplates and a Faraday rotator, (c) Heat map of the total cost function Y as a function of input polarization (A_x, φ) for an optimized PC setting, (d) Heat map of the total cost function Y as a function of the PC setting $(\vartheta_1, \vartheta_2)$ for a fixed diagonal input polarization.

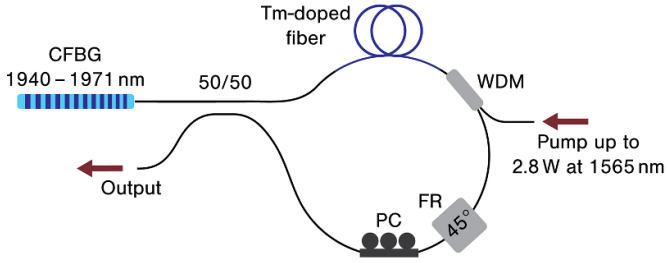

Figure 3. Experimental setup of the figure-of-9 thulium doped fiber laser cavity.

3. Experiment

3.1. Setup

Figure 3 depicts a schematic of the figure-of-9 laser source that we developed. It consists of a phase-shifted NALM (as previously described) in combination with a CFBG. For the NALM, we used a 2.5 m long Tm^{3+}-doped active fiber (OFS TmDF200) that is pumped through a WDM with up to 2.8 W of pump power at 1565 nm wavelength. The other port of the WDM is connected to a FR, which rotates the passing polarization clockwise by 45° and is fiber-coupled to single-mode fiber pigtails. On the other end, the FR is combined with a large-paddle PC, which is again connected to the 50/50 coupler. To stabilize the emission wavelength of the laser cavity, we connect the other side of the output coupler to the CFBG. In order to allow the formation of sub-ps pulses with a broad optical spectrum, the CFBG is fabricated such that its reflectivity is more than 90% from 1940.2 nm to 1971.4 nm as seen in figure 4(a) (blue trace). The grating was inscribed into the core of a Ge-doped silica fiber using a phase mask in combination with femtosecond laser pulses [28]. The grating is 15 mm long with a central grating period of 678 nm and a chirp rate of 9.35 nm cm^{-1}. As a result, the CFBG adds a negative dispersion of –7.6 ps^2 to the laser cavity, in addition to the –1.5 ps^2 from the group velocity dispersion of the optical fibers. The NALM has a total length of 14.4 m, while the fiber containing the CFBG and the top left pigtail of the 50/50 coupler is 2.0 m long. Consequently, the complete resonator length amounts to 18.4 m.

The laser output is obtained from the remaining port of the 50/50 fiber optic coupler and monitored using a power meter, an optical spectrum analyzer (OSA), an optical autocorrelator, and a 22 GHz photodetector in combination with an oscilloscope and an electrical spectrum analyzer (ESA).

3.2. Results

We originally built the laser cavity without the FR, i.e. without a NRPS. We progressively raised the pump power from 1.0 W to 2.6 W while adjusting the PC paddle settings. Yet, we found no evidence of mode-locking or Q-switching. We, therefore, incorporated the FR into the laser cavity to induce a nonreciprocal phase shift of 180°. We increased the pump power while also adjusting the PC paddles. At 2.6 W of pump power and after carefully setting the PC paddles, we observed a self-starting mode-locked pulse train. To improve the stability of the pulse train, we raised the pump power to 2.8 W, but avoided further increments to prevent the fiber optical components from potential damage.

The red trace in figure 4(a) shows the optical spectrum of the laser output, which is 8.1 nm wide (full width at half maximum, FWHM), centered around 1948.1 nm, and does not show Kelly sidebands, which is further discussed in section 3.3. According to prior investigations, lasing occurs on the short-wavelength side of the CFBG reflection window because the Tm^{3+} emission cross increases towards its maximum at 1930 nm [29]. We validated the presence of sub-ps laser pulses using the intensity autocorrelation measurement shown in figure 4(b). We fitted the autocorrelation for a $sech^2$ pulse shape and obtained a pulse width of 560 fs. Together with the width of the optical spectrum, this yields a time-bandwidth product of 0.358, which is 14% above the Fourier transform limit. The presence of a fundamentally

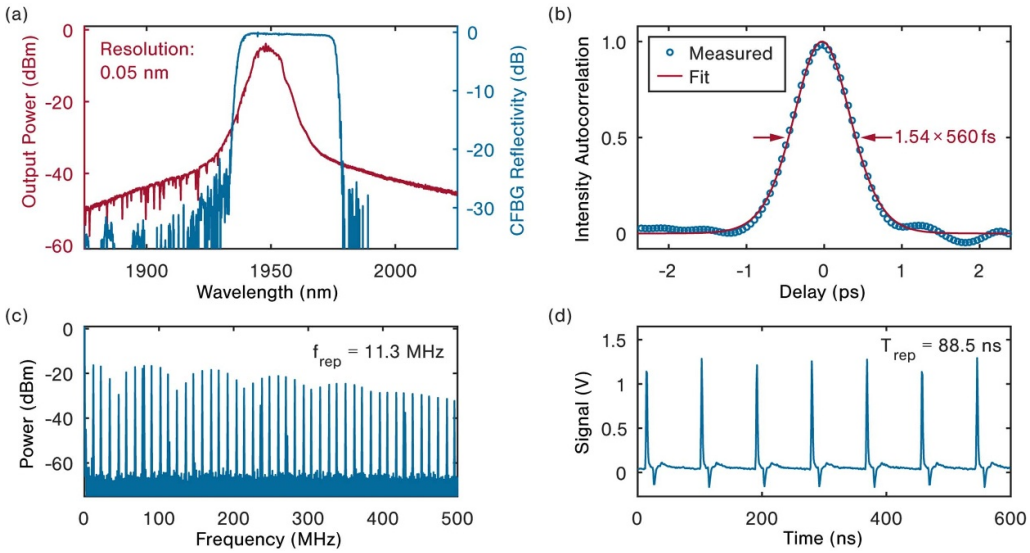

Figure 4. (a) Optical output spectrum (red) and CFBG reflectivity (blue) as a function of wavelength, (b) measured pulse autocorrelation and corresponding sech^2 fit, (c) measured RF spectrum, (d) measured pulse train.

mode-locked pulse train was further confirmed using the ESA. The radio-frequency spectrum shown in figure 4(c) consists of equidistant lines separated by the fundamental repetition rate of 11.3 MHz. This number agrees with figure 4(d), which displays a recorded pulse train on the oscilloscope with a repetition period of 88.5 ns. The repetition rate and period are in accordance with the resonator length of 18.4 m per round trip. The laser remained in stable mode-locking for more than two hours, with an average output power of 101 mW ± 23 mW. This corresponds to a peak output power of 16.3 kW ± 3.7 kW. Table 1 summarizes our laser cavity's key figures of merit and compares them to previously reported NALM-based TDFLs.

3.3. Discussion

Our experimental findings are consistent with the theoretical considerations presented in section 2.2. Without the FR to provide the requisite 180° shift to the NALM reflectivity as a function of input power (cf section 2.1), self-starting mode-locking could not be achieved. By incorporating the FR, we reached mode-locking but only for one particular polarization setting.

The laser output wavelength is stabilized at 1948.1 nm. Nevertheless, within the Tm^{3+} gain band, which covers 1.6 µm to 2.1 µm wavelength, the emission wavelength could be easily adjusted by replacing the CFBG [31]. Furthermore, by adding strain to the fiber Bragg grating, the reflection band may be adjusted within an 80 nm range [32]. Combined with the CFBG reflection band, the emission wavelength may therefore be controlled across a wide wavelength range [29, 33].

We report the generation of 560 fs long pulses using our laser cavity. In previous demonstrations, NALM-based TDFLs achieved pulse duration as short as 150 fs, while exhibiting at least two orders of magnitude lower net cavity dispersion (cf table 1). By lowering the cavity dispersion, we should therefore be able to further decrease the pulse duration. The use of a CFBG, in particular, provides an easy technique to approach the net zero-dispersion regime. The dispersion provided by the CFBG can be adjusted by modifying the grating period chirp, and the sign of the chirp can be inverted by flipping the CFBG. As a result, we believe that our approach can be employed to generate even shorter pulses with broader optical spectra than the 8.1 nm (FWHM) reported in this article.

Based on the pulse duration and spectral width, we calculated a time-bandwidth product 14% above the Fourier transform limit, but note the absence of Kelly sidebands in the laser output spectrum. These sidebands are a characteristic phenomenon found in fiber lasers exhibiting negative dispersion, resulting from the interaction of a cavity soliton with its dispersive wave [34–36]. However, it was shown that for laser cavities similar to ours, which incorporate a CFBG in combination with a SA, a CFBG may suppress the dispersive wave on both sides of the laser spectrum, preventing the formation of Kelly sidebands [37]. We therefore attribute the non-occurrence of Kelly sidebands to the overlap between the laser output spectrum and the CFBG reflection band.

Finally, the pump power threshold required to observe passive mode-locking was found to be 2.6 W. This value surpasses that of comparable TDFLs (cf table 1), which may be attributed to the longer pulse duration. Chernysheva *et al* [30] reports a conversion of 10.6% of pump power at the same pump wavelength, which is three times higher than in our case (3.4%). This is probably due to our low repetition rate of 11.3 MHz in combination with the forced operation of our laser at 1948 nm wavelength, which is around 100 nm beyond the maximal gain of our thulium-doped fiber at 1850 nm wavelength. While we think that the efficiency could be enhanced by increasing the repetition rate, we nevertheless report a high output power of 101 mW together with a substantially higher peak power of 16.3 kW.

Table 1. Comparison of our laser cavity to previously studied NALM-based TDFLs by employed component for self-starting, net cavity dispersion (NCD), pump power threshold for passive mode-locking (P_{th}), repetition rate (f_{rep}), pulse length (T_{pulse}), average output power ($P_{av,out}$), and output peak power ($P_{out,peak}$).

Reference	Component for self-starting	NCD (ps^2)	P_{th} (W)	f_{rep}(MHz)	T_{pulse} (fs)	$P_{av,out}$(mW)	$P_{out,peak}$(kW)
[22]	Free-space NRPS	0.02	0.70	72	250–270	6	0.3
[23]	Free-space NRPS	–0.006	0.80	60	152–483	30	1.0–3.3
[24]	Additional CNTs	–0.093	<0.36	46	450	18	0.6
[30]	Additional SESAM	–0.031	<0.31	53	230	107	3.7
This work	All-fiber NRPS	–9.1	2.60	11	560	101	16.3

4. Conclusion

We demonstrate an all-fiber figure-of-9 mode-locked TDFL that combines an artificial SA (NALM) with a CFBG as a wavelength-selective mirror. Because of a nonreciprocal phase-shifter in the NALM, our laser self-started mode-locking at 1948.1 nm wavelength. Overall, we presented for the first time a straightforward method to generate sub-ps pulses at a controlled wavelength inside the 2 μm band that does not require free-space components or a material SA that degrades over time. Our findings open the way for the development of a supercontinuum or frequency comb source for 2 μm spectroscopic applications.

Conflict of interest

The authors declare that they have no known competing financial interests or personal relationships that could have appeared to influence the work reported in this paper.

Funding

This research was funded by the European Commission (H2020 Marie Skłodowska-Curie Actions, 861 152), the German Research Council (GRK 2101, NO 462/18-1), the German Federal Ministry for Economic Affairs and Climate Action (ZF4309605DF9), and the Swiss National Science Foundation (20 0021 L-182 414).

References

[1] Gordon I E *et al* 2017 The HITRAN2016 molecular spectroscopic database *J. Quant. Spectrosc. Radiat. Transfer* **203** 3–69
[2] Geng J, Wang Q and Jiang S 2011 2 μm fiber laser sources and their applications *Nanophotonics and Macrophotonics for Space Environments V* vol 8164 p 816409
[3] Ma J, Qin Z, Xie G, Qian L and Tang D 2019 Review of mid-infrared mode-locked laser sources in the 2.0 μm–3.5 μm spectral region *Appl. Phys. Rev.* **6** 21317
[4] Popa D and Udrea F 2019 Towards integrated mid-infrared gas sensors *Sensors* **19** 2076
[5] Uliel Y, Cohen-Elias D, Sicron N, Grimberg I, Snapi N, Paltiel Y and Katz M 2017 InGaAs/GaAsSb Type-II superlattice based photodiodes for short wave infrared detection *Infrared Phys. Technol.* **84** 63–71
[6] Keller U, Weingarten K J, Kärtner F X, Kopf D, Braun B, Jung I D, Fluck R, Hönninger C, Matuschek N and Aus Der Au J 1996 Semiconductor saturable absorber mirrors (SESAM's) for femtosecond to nanosecond pulse generation in solid-state lasers *IEEE J. Sel. Top. Quantum Electron.* **2** 435–51
[7] Song Y-W, Yamashita S, Goh C S and Set S Y 2007 Carbon nanotube mode lockers with enhanced nonlinearity via evanescent field interaction in D-shaped fibers *Opt. Lett.* **32** 148
[8] Kieu K and Mansuripur M 2007 Femtosecond laser pulse generation with a fiber taper embedded in carbon nanotube/polymer composite *Opt. Lett.* **32** 2242
[9] Popa D, Sun Z, Torrisi F, Hasan T, Wang F and Ferrari A C 2010 Sub 200 fs pulse generation from a graphene mode-locked fiber laser *Appl. Phys. Lett.* **97** 1–4
[10] Kim J and Song Y 2016 Ultralow-noise mode-locked fiber lasers and frequency combs: principles, status and applications *Adv. Opt. Photon.* **8** 465
[11] Mayer A S *et al* 2020 Flexible all-PM NALM Yb:fiber laser design for frequency comb applications: operation regimes and their noise properties *Opt. Express* **28** 18946
[12] Viskontas K, Regelskis K and Rusteika N 2014 Slow and fast optical degradation of the SESAM for fiber laser mode-locking at 1 μm *Lith. J. Phys.* **54** 127–35
[13] Ryu S Y, Kim K-S, Kim J and Kim S 2012 Degradation of optical properties of a film-type single-wall carbon nanotubes saturable absorber (SWNT-SA) with an Er-doped all-fiber laser *Opt. Express* **20** 12966
[14] Kuse N, Jiang J, Lee C-C, Schibli T R and Fermann M E 2016 All polarization-maintaining Er fiber-based optical frequency combs with nonlinear amplifying loop mirror *Opt. Express* **24** 3095–102
[15] Nicholson J W and Andrejco M 2006 A polarization maintaining, dispersion managed, femtosecond figure-eight fiber laser *Opt. Express* **14** 8160
[16] Michalska M 2021 Dispersion managed thulium-doped fiber laser mode-locked by the nonlinear loop mirror *Opt. Laser Technol.* **138** 106923
[17] Kim D, Kwon D, Lee B and Kim J 2019 Polarization-maintaining nonlinear-amplifying-loop-mirror mode-locked fiber laser based on a 3 × 3 coupler *Opt. Lett.* **44** 1068
[18] MenloSystems 2013 Laser with non-linear optical loop mirror *European Patent* EP2637265A1 European Patent Office
[19] Lin H, Donald D K and Sorin W V 1994 Optimizing polarization states in a figure-8 laser using a nonreciprocal phase shifter *J. Lightwave Technol.* **12** 1121–8
[20] Jiang T, Cui Y, Lu P, Li C, Wang A and Zhang Z 2016 All PM fiber laser mode locked with a compact phase biased amplifier loop mirror *IEEE Photonics Technol. Lett.* **28** 1786–9
[21] Hänsel W *et al* 2017 All polarization-maintaining fiber laser architecture for robust femtosecond pulse generation *Appl. Phys.* B **123** 41
[22] Liao R, Song Y, Liu W, Shi H, Chai L and Hu M 2018 Dual-comb spectroscopy with a single free-running thulium-doped fiber laser *Opt. Express* **26** 11046

[23] Liao R, Song Y, Chai L and Hu M 2019 Pulse dynamics manipulation by the phase bias in a nonlinear fiber amplifying loop mirror *Opt. Express* **27** 14705
[24] Chernysheva M A, Krylov A A, Kryukov P G, Arutyunyan N R, Pozharov A S, Obraztsova E D and Dianov E M 2012 Thulium-doped mode-locked all-fiber laser based on NALM and carbon nanotube saturable absorber *Opt. Express* **20** B124–30
[25] Doran N J and Wood D 1988 Nonlinear-optical loop mirror *Opt. Lett.* **13** 56
[26] Fermann M E, Haberl F, Hofer M and Hochreiter H 1990 Nonlinear amplifying loop mirror *Opt. Lett.* **15** 752
[27] Duling I N, Chen C-J, Wai P K and Menyuk C R 1994 Operation of a nonlinear loop mirror in a laser cavity *IEEE J. Quantum Electron.* **30** 194–9
[28] Goebel T A, Heusinger M, Krämer R G, Matzdorf C, Imogore T O, Richter D, Zeitner U D and Nolte S 2020 Femtosecond inscription of semi-aperiodic multi-notch fiber Bragg gratings using a phase mask *Opt. Express* **28** 35682
[29] Bartnick M, Bharathan G, Goebel T A, Krämer R G, Nolte S and Brès C-S 2022 Wavelength-stabilized tunable mode-locked thulium-doped fiber laser beyond 2 μm *Opt. Lett.* **47** 2085
[30] Chernysheva M A, Krylov A A, Kryukov P G and Dianov E M 2012 Nonlinear amplifying loop-mirror-based mode-locked thulium-doped fiber laser *IEEE Photonics Technol. Lett.* **24** 1254–6
[31] Bartnick M, Bharathan G, Lago-Rached L, Mussot A and Brès C-S 2022 Wavelength-stabilized mode-locked thulium-doped fiber laser operating between 1958 and 2008 nm *Conf. on Lasers and Electro-Optics* (Science and Innovations) Paper SM5L.3 (https://doi.org/10.1364/CLEO_SI.2022.SM5L.3)
[32] Bélanger E, Déry B, Bernier M, Bérubé J-P and Vallée R 2007 Long-term stable device for tuning fiber Bragg gratings *Appl. Opt.* **46** 3189–95
[33] Bharathan G, Woodward R I, Ams M, Hudson D D, Jackson S D and Fuerbach A 2017 Direct inscription of Bragg gratings into coated fluoride fibers for widely tunable and robust mid-infrared lasers *Opt. Express* **25** 30013
[34] Kelly S M J 1992 Characteristic sideband instability of periodically amplified average soliton *Electron. Lett.* **28** 806–7
[35] Noske D U, Pandit N and Taylor J R 1992 Source of spectral and temporal instability in soliton fiber lasers *Opt. Lett.* **17** 1515
[36] Dennis M L and Duling I N 1994 Experimental Study of Sideband Generation in Femtosecond Fiber Lasers *IEEE J. Quantum Electron.* **30** 1469–77
[37] Han D and Liu X 2012 Sideband-controllable mode-locking fiber laser based on chirped fiber Bragg gratings *Opt. Express* **20** 27045